RESEARCH ARTICLE

High-Efficiency (Over 10%) Parallel Tandem Dye-Sensitized Solar Cells Based on Tri-Carbon Electrodes

Wu Shao[1] · Wenjun Wu[1]

Abstract

Ensuring high power conversion efficiency, partially or completely replacing Pt electrodes with inexpensive materials is one of the important development directions of dye-sensitized solar cells (DSSCs). In this work, we have developed a three-component (MWCNTs, carbon black and graphite) carbon (tri-carbon) electrode material for DSSC devices combined with the advantages of high electron transfer kinetics of MWCNTs, plentiful catalytic sites in crystal edges of carbon black and superior electrical conductivity and catalytic activity of graphite. Using a tri-carbon electrode, a Pt electrode, and two N719-sensitized photoanodes, a parallel tandem dye-sensitized solar cells are assembled obtaining a high PCE of 10.26% ($V_{oc} = 0.70$ V, $J_{sc} = 19.99$ mA/cm^2, FF = 73.33%). It opens up a new avenue for the development of low-cost and high-performance DSSCs.

Keywords Dye-sensitized solar cells · MWCNTs · Carbon black · Graphite · Counter electrode

Introduction

Dye-sensitized solar cells (DSSCs) are considered one of the most promising photovoltaic devices to replace traditional silicon-based solar cells because of their low cost, simple fabrication, high conversion efficiency, and environmental friendliness [1, 2]. Its counter electrode, in particular, is an important component for enriching electrons in the external circuit and transferring them to the electrolyte to realize its reduction and regeneration [3]. As a conventional counter electrode material for DSSCs, platinum demonstrates excellent conductivity and catalytic performance. However, due to its valuableness and easy reaction with iodide under irradiation, it is not conducive to the sustainable development of DSSCs [4, 5]. Therefore, identifying non-platinum materials with low prices and excellent catalytic performance is necessary. Until now, nanocarbon has been developed as one of the most promising materials.

Carbon nanotubes (CNTs) are nanoscale carbon materials with high stability, chemical resistance, electrical conductivity, and surface area. CNTs are categorized into single-walled carbon nanotubes (SWCNTs) and multi-walled carbon nanotubes (MWCNTs). SWCNTs consist of single rolling graphene sheets, while MWCNTs contain numerous coaxially aligned graphene sheets. Using N719 as a sensitizer, SWCNTs and MWCNTs as a counter electrode for DSSC, a power conversion efficiency (PCE) of 4.5% [6] and 7.7% [7–10] can be obtained, respectively. The higher PCE of MWCNTs can be attributed to their excellent electron transfer kinetics (low charge transfer resistance). Carbon black also exhibits high triiodide catalytic performance as a platinum-free counter electrode of DSSCs due to its numerous catalytic active sites in its crystalline edges. With a carbon black film thickness of 10 μm (the greater thickness, the lower charge transfers resistance (R_{ct})), the optimal PCE can be enhanced to 9.1% ($J_{sc} = 16.8$ mA/cm^2, $V_{oc} = 789.8$ mV, fill factor (FF) = 0.685) [11].

Graphite, another allotrope of carbon, is an interesting catalyst and conductive layer material that occurs naturally. Graphite materials are typically made up of basal and edge planes. The basal planes exhibit slow electron transport, while the edge planes exhibit fast electron transport [12]. Rhee et al. [13] used submicron-sized colloidal graphite (CG) as a catalytic material for I_3^- reduction in DSSC

✉ Wenjun Wu
  wjwu@ecust.edu.cn

[1] Key Laboratory for Advanced Materials and Feringa
  Nobel Prize Scientist Joint Research Center, Shanghai Key
  Laboratory of Functional Materials Chemistry, East China
  University of Science and Technology, Shanghai 200237,
  China

Scheme 1 Schematic diagram of the parallel tandem DSSC based on tri-carbon and Pt electrodes
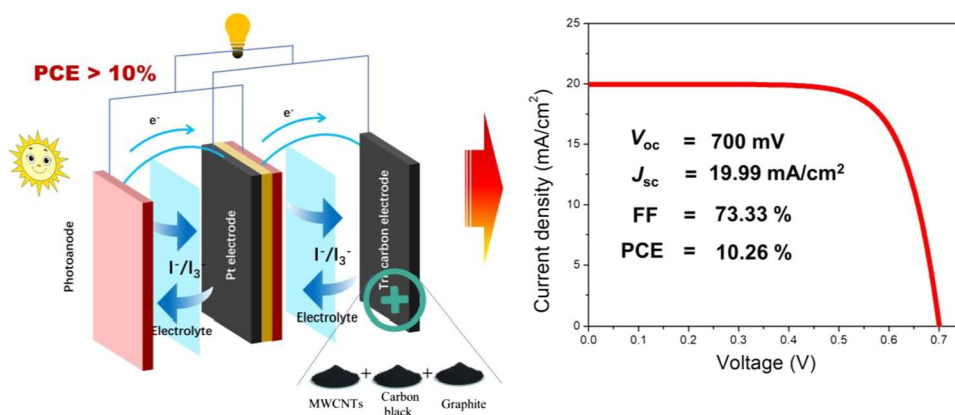
instead of Pt electrodes. They discovered that the charge transfers resistance decreases as the graphite layer thickness increases from 3 to 9 μm. Furthermore, they found that under 100 mW/cm^2, and AM 1.5 simulated sunlight, submicron-sized CG showed an energy conversion efficiency greater than 6.0%, which is comparable to that of Pt. Han et al. [14] developed a mesoscopic platinized graphite/carbon black counter electrode for DSSC. The carbon electrode loaded with 0.5% Pt showed significantly improved catalytic activity and charge transfer rate. Additionally, they obtained a high energy conversion efficiency of 7.61% for DSSCs.

However, due to the translucency of the dye-sensitized photoanode and Pt counter electrode, a significant amount of light is lost during the testing process. The assembly of tandem-structured devices is an effective way to make full use of incident light and improve photovoltaic performance, including series and parallel modes. The most noticeable advantage of using series mode is the significant increase in the open-circuit voltage [15]. A 10.4% PCE was obtained by fabricating a series of tandem devices based on two Pt counter electrodes, an N719 top cell, and a black-dye bottom cell, and the open-circuit voltage (V_{oc}) reached 1.45 V [16], while for the parallel mode, it is better to lift the J_{sc} of DSSCs. Further, Sugihara et al. [17] assembled the tandem DSSCs in parallel mode with an N719 top cell and black-dye bottom device based on Pt counter electrodes. The certified PCE can reach 10.6%, with a short-circuit current density (J_{sc}) of up to 20.0 mA/cm^2.

Here, we developed a three-component carbon (tri-carbon) electrode material for DSSC devices combined with the advantages of high electron transfer kinetics of MWCNTs, plentiful catalytic sites in the crystal edges of carbon black, and superior electrical conductivity and catalytic activity of graphite. Using a tri-carbon electrode, a Pt electrode, and two N719-sensitized photoanodes, a parallel tandem DSSC (shown in Scheme 1) was assembled to obtain a high PCE of 10.26% (V_{oc} = 0.70 V, J_{sc} = 19.99 mA/cm^2, FF = 73.33%). This opens up a new avenue for developing low-cost and high-performance DSSCs.

Experimental Section

Materials

Fluorine-doped tin (FTO) conductive glass (FTO surface layer, visible light transmittance > 85%, sheet resistance 7 ± 1.5 Ω) was purchased from Yingkou Opvtech New Energy Technology Co., Ltd., China; 1-butyl-3-methyl-imidazolium iodide (BMII) was purchased from Sigma-Aldrich; di-tetrabutylammonium-bis(isothiocyano) bis(2,2'-bipyridine-4,4'-dicarboxy)ruthenium (N719), 18-NRT transmission layer, and 18NR-AO scattering layer TiO$_2$ paste were purchased from Greatcellsolar Company, Australia; lithium iodide was obtained from Fluka; iodine (99.999%) was obtained from Alfa Aesar; chloroplatinic acid and industrial-grade MWCNT were obtained from Shanghai McLean Biochemical Technology Co., Ltd.; carbon black (CB) and micron graphite (MG, 2000 mesh) were obtained from Shanghai Aladdin Biochemical Technology Co., Ltd.; and ethyl cellulose (45–55 mPa·s) was obtained from Beijing J&K Scientific Co., Ltd. All reagents were of AR grades and used directly without further processing.

Device Characterization

The morphology of the devices was observed using field emission scanning electron microscopy (FESEM; ThermoFisher Talos F200X, 200 kV). The photocurrent density–voltage characteristics were measured using a Keithley 2400 source meter under air mass (AM) 1.5 illumination at 100 mW/cm^2 using an Oriel 91106 solar simulator (Newport, USA) with a scan rate of 20 mV/s. Next, the active area of the device was approximately 0.25 cm^2, and a mask with an oblong aperture (0.0875 cm^2) was applied under J–V tests. The incident photon-to-electron conversion efficiency (IPCE) spectra were recorded using

the Newport-74125 system (Newport Instruments). Electrochemical impedance spectroscopy (EIS) was performed on ZAHNER ENNIUM electrochemical workstations in the frequency range from 1 to 3.92 MHz.

Preparation of Counter Electrode

Tri-Carbon Electrode

The tri-carbon paste was obtained using a planetary ball mill with a 0.45 g mixture of MWCNT, MG, and CB in a different mass ratio, and 0.055 g ethylcellulose and 2.0 g terpineol for 48 h. Next, a thin tri-carbon film was obtained on the cleaned FTO conductive glass by screen printing technology and calcined at 400 °C for 30 min. Similarly, single MWCNT, CB, and MG counter electrodes were prepared.

Pt Electrode

Some isopropanol solutions of chloroplatinic acid (0.02 mol/L) were added dropwise to the cleaned FTO conductive glass using a spin coating (2000 r/min), and a thin film of Pt was formed after calcining at 400 °C for 15 min.

Preparation of Liquid Electrolyte

0.5 mol/L tetra-butylpyridine (TBP), 0.05 mol/L iodine, 0.1 mol/L lithium iodide, 0.1 mol/L 1,3-dimethyl-3-propylimidazolium iodide (DMPII), 0.6 mol/L 1-butyl-3-methylimidazolium iodide (BMII), and 0.1 mol/L guanidinium thiocyanate (GuSCN) were dissolved in a mixture of acetonitrile and valeronitrile (85:15, V:V).

Preparation of TiO$_2$ Photoanode

Titanium dioxide paste of 18NR-T and 18NR-AO was deposited onto clean FTO conductive glass using screen printing, respectively. The TiO$_2$ electrodes (area = 0.25 cm^2) were gradually heated in a muffle furnace with the programmed temperature of 325 °C for 5 min, 375 °C for 5 min, 450 °C for 15 min, and 500 °C for 15 min. The TiO$_2$ electrodes were cooled to room temperature, treated with a dilute solution of TiCl$_4$ (40 mmol/L, 75 °C for 30 min), and sintered at 500 °C for 30 min. The electrodes were allowed to cool (80–100 °C) and immersed in an N719 (3 mmol/L) ethanol solution overnight.

Results and Discussion

Electrode Morphology Characterization

The microstructures of tri-carbon, MWCNT, CB, and MG electrode materials were obtained using FESEM (Fig. 1). Micron-sized MWCNTs, CB, and MG are uniformly interwoven together for the tri-carbon material, as shown in Fig. 1a. Compared with Fig. 1b (MWCNTs) and Fig. 1c (CB), MWCNTs and CB maintained their original morphology in tri-carbon. MWCNT, for example, demonstrates a tubular structure that improves electron transport and a

Fig. 1 Field emission scanning electron microscopy (FESEM) images of **a** tri-carbon, **b** MWCNT, **c** CB, and **d** MG counter electrodes
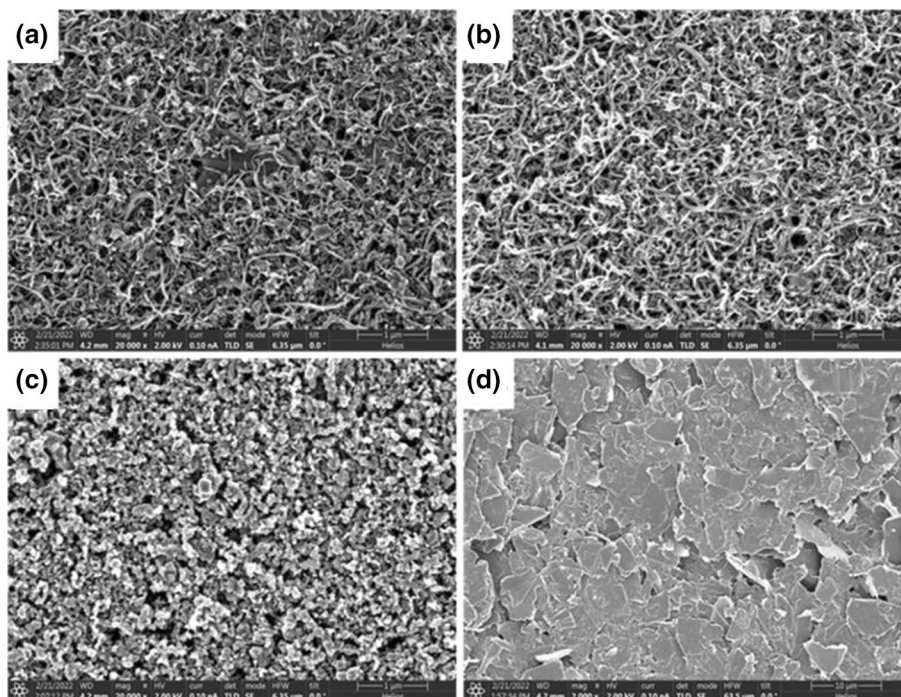
rough surface that enables the adhesion of additional electrolytes [18, 19]. CB demonstrates a more uniform granular structure, resulting in a larger specific surface area. Furthermore, when compared with Fig. 1d (MG), the area of the MG sheets in the tri-carbon is significantly smaller due to the mutual shearing effect of the three components, which allows the lamellar graphite to display more defect sites and provides more catalytic active sites. However, the interwoven structure of tri-carbon significantly increases the specific surface area of the electrode and the contact area between the electrolyte and counter electrode, which is more conducive to the regeneration of the I_3^- than single MWCNT, CB, or MG. Furthermore, a significant number of MWCNTs interspersed inside the carbon electrode also contribute to the conduction of electrons inside the electrode.

Influence of the Mass Ratio of MWCNT/MG/CB on the Photovoltaic Performance of the Device

According to reference [14], the mass ratio of 3:1 for graphite to CB was chosen as the suitable ratio in this work because it demonstrates the lowest sum of sheet resistance and charge transfer resistance. Next, to maximize the synergistic catalytic effect of the compound based on MWCNT, MG, and CB, their optimal mass ratio was screened using optoelectronic properties by setting the mass ratio of MG/CB to 3:1 and varying the amount of MWCNT used here. The mass ratios of MWCNT/MG/CB were chosen to be 0:3:1, 1:3:1, 2:3:1, 6:3:1, 10:3:1, 14:3:1, and 18:3:1. Figure 2 and

Table 1 show the specific photovoltaic parameters following with mass ratio.

As shown in Fig. 2 and Table 1, the ratio of MWCNT/MG/CB increases from 0:3:1 to 18:3:1, and the J_{sc} (Fig. 2a) and FF (Fig. 2c) increase first with an increase in the amount of MWCNT and then decrease. The optimal ratio obtained was T3 (6:3:1) with the highest PCE (8.30%). However, the open-circuit voltage hardly changed from T0 to T6. The increase in J_{sc} and FF with increasing MWCNT may be due to the improvement of charge transfer performance inside the electrode using MWCNT as electronic wires. Next, when the usage of MWCNTs continued to increase beyond 6:3:1, the contact between CB and graphite was isolated, and the conductivity of graphite was reduced, inducing the degradation of photoelectric conversion performance [20]. Further parallel comparison of photovoltaic parameters in Fig. 2 and

Table 1 Photovoltaic parameters of DSSCs with different ratios of MWCNT, MG, and CB

Sample	Ratio	V_{oc}(V)	J_{sc} (mA/cm^2)	FF (%)	PCE (%)
T0	0:3:1	0.68	16.53	60.28	6.81
T1	1:3:1	0.68	16.34	61.53	6.81
T2	2:3:1	0.69	16.84	62.71	7.24
T3	6:3:1	0.68	18.20	66.87	8.30
T4	10:3:1	0.70	16.49	61.64	7.08
T5	14:3:1	0.70	16.05	61.55	6.89
T6	18:3:1	0.69	15.54	60.19	6.43

Fig. 2 Photovoltaic parameters **a** photocurrent, **b** voltage, **c** FF, and **d** PCE curves based on the different ratios of MWCNT, MG, and CB
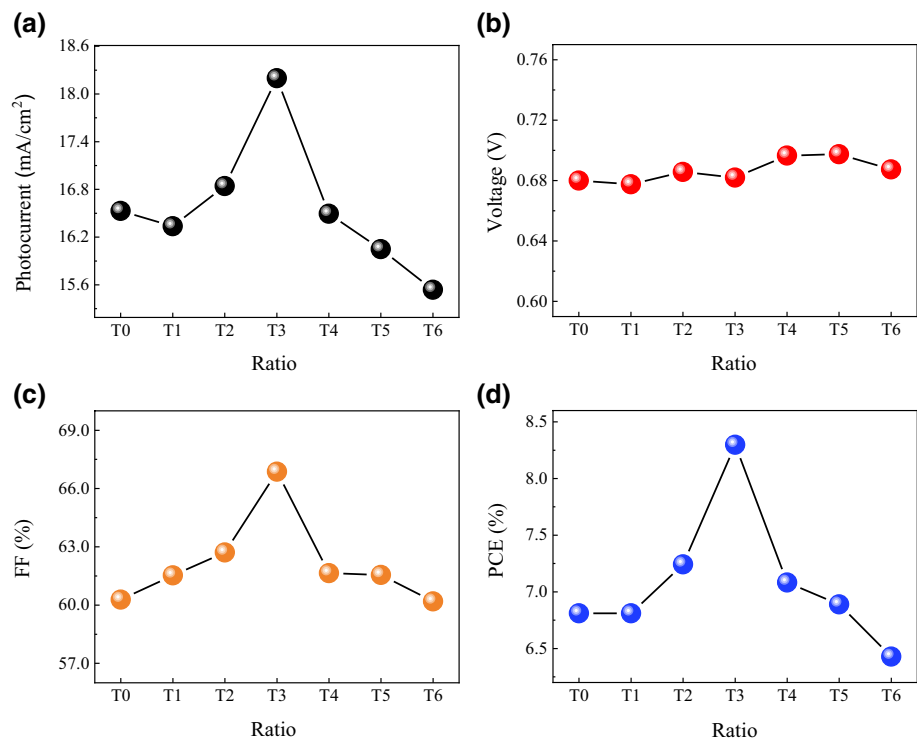
Table 1 reveals that J_{sc} current and FF are the main factors influencing PCE.

Single and Tandem DSSCs with Different Counter Electrodes

To fully use the large amount of sunlight lost through the translucent TiO_2 photoanode and Pt counter electrode for secondary photoelectric conversion, a parallel tandem DSSC was assembled using both Pt and tri-carbon electrodes (shown in Scheme 1) with N719 as a sensitizer. Figure 3 presents the J–V characteristic curves of the assembled single DSSCs (MWCNT, CB, MG, and Pt) and tandem DSSCs (Pt + tri-carbon). Next, Table 2 lists the specific photovoltaic performance parameters, including V_{oc}, J_{sc}, FF, and PCE.

As depicted in Fig. 3 and Table 2, for single DSSCs, the order of PCE for different counter electrodes is Pt (9.68%) > tri-carbon (8.30%) > MWCNT (6.92%) > CB (6.65%) > MG (6.39%). Under the same conditions, different carbon materials demonstrate differences in structure and performance. MWCNT, CB, and graphite were in the form of tubular morphology, fine particles, and lamellar structure, respectively. Therefore, the corresponding J_{sc} and FF differ slightly, but they exhibit a little effect on the photoelectric properties, while MWCNT demonstrates a slight advantage. The PCE of tri-carbon was significantly improved due to the synergistic effect of MWCNT, CB, and MG, reaching 8.30% (V_{oc} = 0.68 V, J_{sc} = 18.20 mA/cm², and FF = 66.87%), owing mostly to the enhancement of J_{sc} and FF. Compared with MWCNT, CB, and MG, the J_{sc} and FF were improved from 16.19 mA/cm² and 63.44%, 15.85 mA/cm² and 60.94%, 17.84 mA/cm² and 52.40% to 18.20 mA/cm² and 66.87%,

Table 2 The photoelectric parameters of single DSSCs (Tri-carbon, MWCNT, CB, MG, and Pt) and tandem devices (Pt + tri-carbon)

| CE	V_{oc} (V)	J_{sc} (mA/cm²)	FF	PCE (%)
Pt	0.69	19.37	71.94	9.68
Tri-carbon	0.68	18.20	66.87	8.30
MWCNT	0.67	16.19	63.44	6.92
CB	0.69	15.85	60.94	6.65
MG	0.68	17.84	52.40	6.39
Pt + tri-carbon	0.70	19.99	73.33	10.26

respectively. Meanwhile, based on the tri-carbon electrode, its J_{sc} is comparable to that of Pt (19.37 mA/cm²).

The PCE of tandem DSSC Pt + tri-carbon was as high as 10.26% due to the bottom cell's full usage of transmitted light. The J_{sc} and FF were close to 20 mA/cm² and 73.33%, respectively, with a parallel mode used.

In Fig. 4, to characterize the photoelectric conversion performance of the devices for different wavelengths of light, the incident monochromatic IPCE is an important parameter. It is defined as the ratio of photocurrent density to incident light flux in an external circuit. Generally, the integral of the IPCE value over the wavelength (300–850 nm) represents the J_{sc} when its light intensity is scaled up to reach the standard light intensity. That is to say that it can obtain higher J_{sc} under white light with higher IPCE values and a wider spectrum. Since all photoanodes use N719 as a sensitizer, the six device groups (tri-carbon, MWCNT, CB, MG, Pt, and Pt + tri-carbon as counter electrodes) do not show obvious spectral differences except in the magnitude of the IPCE values. Additionally, the order of the maximum IPCE value is Pt (90.2%) > Pt + tri-carbon (89.2%) > tri-carbon
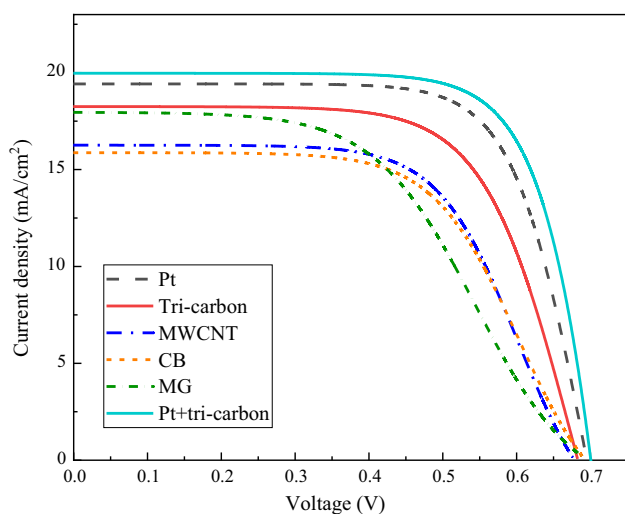
Fig. 3 The J–V curves of single DSSCs (tri-carbon, MWCNT, CB, MG, and Pt) and tandem devices (Pt + tri-carbon)
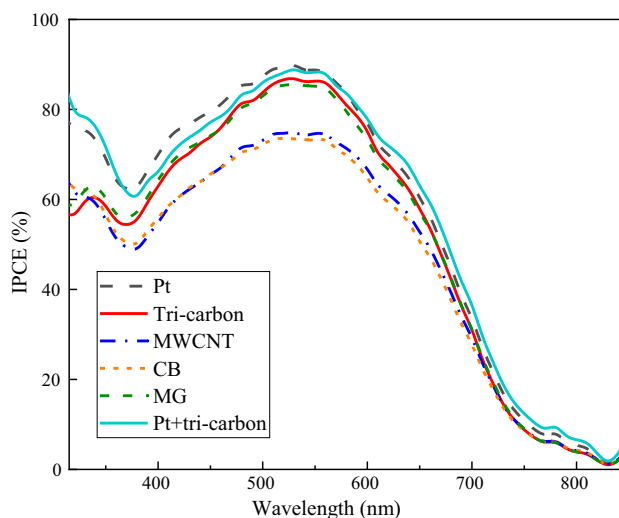
Fig. 4 The IPCE curves of single DSSCs (tri-carbon, MWCNT, CB, MG, and Pt) and tandem devices (Pt + tri-carbon)

(87.0%) > MG (85.6%) > MWCNT (75.1%) > CB (73.6%), almost consistent with the order of J_{sc} in Table 2. Compared with Pt, the maximum IPCE value of Pt + tri-carbon was slightly lower. However, the device based on Pt + tri-carbon obtained a higher J_{sc} due to the slightly broader spectrum. The corresponding integrated photocurrents are as follows: Pt + tri-carbon (19.19 mA/cm^2) > Pt (17.83 mA/cm^2) > tri-carbon (17.12 mA/cm^2) > MG (15.63 mA/cm^2) > MWCNT (14.52 mA/cm^2) > CB (14.27 mA/cm^2). Furthermore, they are consistent with the order of J_{sc} in Table 2.

Conductivity of Different Counter Electrodes

The electrolyte plays the role of transmitting electrons in DSSC. In the reaction with the counter electrode, I_3^- decomposes into I_2 and I^-, which usually reacts rapidly and is considered to be in equilibrium. The iodine reduction reaction at the liquid–solid interface is the decisive step of the counter electrode. That is, the I_2 adsorbed decomposes into iodine atoms on the electrode surface and then electrons are obtained to form solvated I^- [21, 22]. Next, to further compare the efficiency limitations of DSSCs with different counter electrodes, we also measured the conductivity of symmetric cells made of two identical Pt, tri-carbon, MWCNT, CB, or MG electrodes with I^-/I_3^- electrolyte as a function of temperature (in Fig. 5). As shown in Fig. 5, the corresponding curves of ln σ and 1000/T follow the Arrhenius relation, which is a typical ionic conduction behavior catalyzed by these materials. The slope of the measured value varies with temperature for different electrodes with the same electrolyte due to the different catalytic capabilities for I_3^- reduction and electronic conductivity.
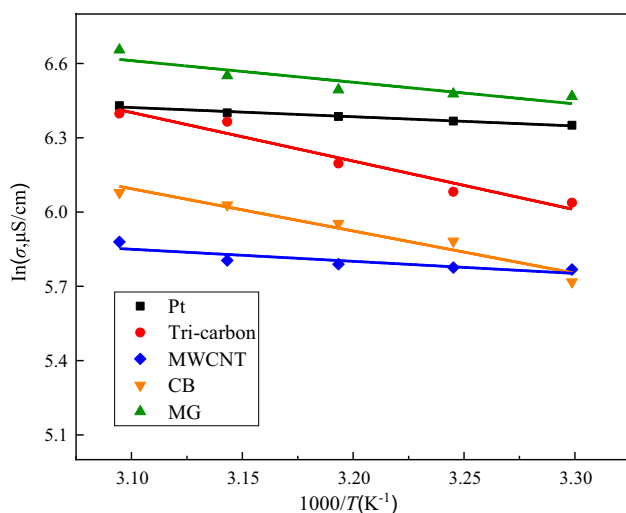
MG demonstrates the highest electrical conductivity, even over a Pt electrode, and its J_{sc} exceeds that of MWCNT and CB (in Table 2), indicating its abundant catalytic sites. Furthermore, the electrical conductivity of the tri-carbon electrode composited with MWCNT, CB, and MG is lower than that of Pt but higher than that of MWCNT and CB. As the temperature of the tri-carbon approaches 50 °C, its conductivity is comparable to that of Pt, indicating that the increase in surface temperature of the device under irradiation is beneficial to improving the photoelectric conversion performance of tri-carbon in practical applications. Additionally, the changing trend of electrical conductivity with temperature for tri-carbon is nearly identical to that of CB, while the electrical conductivity of Pt, MWCNT, and MG does not change significantly with temperature increase.

Electrochemical Impedance and Catalytic Properties

EIS is one of the most sensitive electrochemical techniques, capable of delivering measurable signal changes resulting from the alteration of materials for electrical devices. It is commonly used to characterize the inhibition of charge recombination for photoanode [23] and the catalytic capability for counter electrodes in DSSCs [24].

Next, to characterize the catalytic performance of the different counter electrodes, two identical counter electrodes are usually used to make a symmetric cell, that is, a virtual cell (counter electrode/electrolyte/counter electrode) for EIS tests. Figure 6 shows the results obtained for the electrode materials Pt, tri-carbon, MWCNT, CB, and MG. (Inset is the equivalent circuit.) The EIS spectrum was fitted using ZSimpWin software, and Table 3 lists the related results obtained.
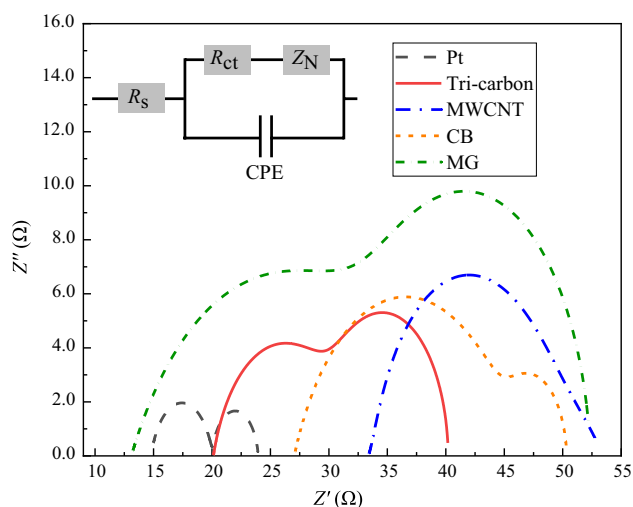

Fig. 5 Conductivity of symmetric cells made of two identical Pt, tri-carbon, MWCNT, CB, and MG electrodes with I^-/I_3^- electrolyte as a function of temperature

Fig. 6 Nyquist plots of the symmetrical cells fabricated with two identical Pt, tri-carbon, MWCNT, CB, and MG electrodes. Inset: equivalent circuit for fitting the impedance spectra

Table 3 Fitted parameters from Nyquist plots of the symmetrical cells with two identical Pt, tri-carbon, MWCNT, CB, and MG electrodes

CE	R_s (Ω)	R_{ct} (Ω)	Z_N (Ω)
Pt	14.80	5.23	3.92
Tri-carbon	20.13	9.31	10.78
MWCNT	33.37	12.06	8.05
CB	27.03	18.79	4.54
MG	13.10	15.90	23.50

As shown in Fig. 6, the intercept of the real axis in the high-frequency region in EIS mainly represents the conductive substrate and electrode material impedance, which is called the series resistance (R_s) [25]. The order of R_s values for the five different electrode materials employed here is the following: MWCNT (33.37 Ω) > CB (27.03 Ω) > tri-carbon (20.13 Ω) > Pt (14.80 Ω) > MG (13.10 Ω). Generally, a smaller R_s results in an improved interface contact between the counter electrode material and the substrate, which benefits the rise of J_{sc}. Particularly for tri-carbon, its R_s is between Pt and CB, which is less than that of MWCNT and CB, indicating that it demonstrates a better charge transport performance than MWCNT and CB.

The fitted diameter of the semicircle in the intermediate frequency region denotes the charge transfer resistance (R_{ct}) between the counter electrode and electrolyte, which is inversely proportional to the catalytic performance of the counter electrode [26]. Additionally, the fitted diameter of the semicircle in the low-frequency region expresses the diffusion impedance (Z_N) of the interface between iodine electrolyte and counter electrode [27]. As shown in Table 3, the R_{ct} of Pt, tri-carbon, MWCNT, CB, and MG is 5.23, 9.31, 12.06, 18.79, and 15.90 Ω, respectively. This proves that the catalytic performance of the composite electrode tri-carbon is lower than that of the Pt electrode, which is consistent with the J–V test results (Fig. 3). For the Z_N values in Table 3, tri-carbon materials got the high Z_N (10.78 Ω), indicating that Z_N is not the limiting factor for the photoelectric conversion process in this system.

Tafel Polarization Properties and Catalytic Activity of Counter Electrode

The Tafel curve, in theory, can be divided into three zones: polarization (distributed over low potential, |Potential |< 120 mV), Tafel (middle potential with a sharp slop), and diffusion (horizontal part) [24, 28].

To explore the effect of different counter electrodes on the charge transfer characteristics, Tafel polarization measurements were performed using dummy cells with two Pt, tri-carbon, MWCNT, CB, and MG electrodes (Fig. 7). In

Fig. 7, the slope of the Tafel polarity is used to evaluate the exchange current density (J_0):

$$J_0 = RT/nFR_{ct}$$

where R is the gas constant; T is the temperature; n is the number of electrons involved in the reaction; and F is the Faraday constant. As depicted in Fig. 7, the slopes of MWCNT and MG are the lowest and nearly identical, while those of tri-carbon are only slightly lower than that of the Pt electrode, indicating superior charge transfer properties. Since J_0 is inversely proportional to R_{ct}, this result is consistent with the calculated result of R_{ct} obtained from the EIS test (Table 3).

The diffusion of ionic carriers in the electrolyte with different electrodes determines transfer resistance limited current density (J_{lim}) for DSSCs, which can be used to evaluate the diffusion rate of ions between two counter electrodes. The J_{lim} obtained from the Tafel diagram is directly proportional to the diffusion coefficient (D_n) of the redox couple (the higher catalytic performance of the counter electrode, the faster diffusion rate).

$$J_{lim} = 2nFCD_n/l$$

where l is the thickness of the spacer; F is the Faraday constant; and C is the electrolyte concentration [29, 30]. In the diffusion zone in Fig. 7, the J_{lim} values lie in the order of Pt > tri-carbon > MWCNT > CB > MG, indicating that tri-carbon can effectively catalyze the reduction of I_3^- and reduce the concentration near the electrode surface due to its high catalytic ability, thereby accelerating the diffusion rate of redox to the electrode surface.
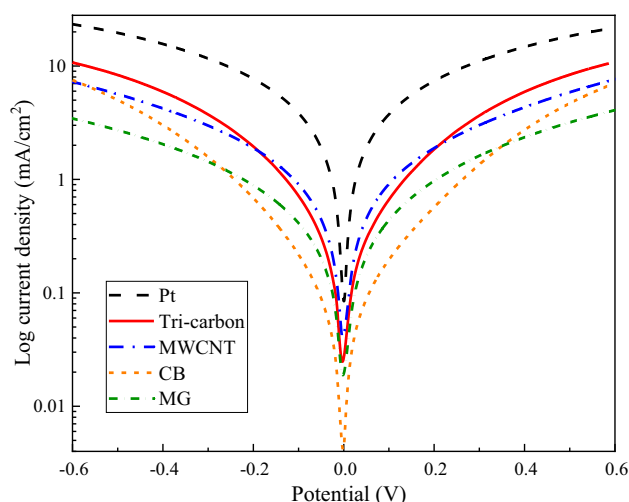
Fig. 7 Tafel polarization curve of symmetrical cells based on Pt, tri-carbon, MWCNT, CB, and MG electrodes

Conclusion

In this work, we developed a three-component carbon electrode material (tri-carbon) with a uniform interwoven structure with MWCNTs, CB, and graphite. Tri-carbon exhibits higher charge transfer qualities and catalytic ability due to the synergistic influence of charge transfer kinetics, catalytic properties of I_3^-, and electrical conductivity. A parallel tandem DSSC is assembled using a tri-carbon electrode, Pt electrode, and two N719-sensitized photoanodes, yielding a high PCE of 10.26% ($V_{oc} = 0.70$ V, $J_{sc} = 19.99$ mA/cm^2, FF = 73.33%).

Declarations

Conflict of interest The authors declare that there is no conflict of interest.

References

1. O'Regan B, Grätzel M (1991) A low-cost, high-efficiency solar cell based on dye-sensitized colloidal TiO₂ films. Nature 353(6346):737–740

2. Yun SN, Qin Y, Uhl AR et al (2018) New-generation integrated devices based on dye-sensitized and perovskite solar cells. Energy Environ Sci 11(3):476–526

3. Karim NA, Mehmood U, Zahid HF et al (2019) Nanostructured photoanode and counter electrode materials for efficient dye-sensitized solar cells (DSSCs). Sol Energy 185:165–188

4. Hagfeldt A, Boschloo G, Sun LC et al (2010) Dye-sensitized solar cells. Chem Rev 110(11):6595–6663

5. Papageorgiou N (2004) Counter-electrode function in nanocrystalline photoelectrochemical cell configurations. Coord Chem Rev 248(13–14):1421–1446

6. Suzuki K, Yamaguchi M, Kumagai M et al (2003) Application of carbon nanotubes to counter electrodes of dye-sensitized solar cells. Chem Lett 32(1):28–29

7. Lee WJ, Ramasamy E, Lee DY et al (2009) Efficient dye-sensitized solar cells with catalytic multiwall carbon nanotube counter electrodes. ACS Appl Mater Interfaces 1(6):1145–1149

8. Lee WJ, Ramasamy E, Lee DY et al (2008) Performance variation of carbon counter electrode based dye-sensitized solar cell. Sol Energy Mater Sol Cells 92(7):814–818

9. Xu SJ, Luo YF, Zhong W (2011) Investigation of catalytic activity of glassy carbon with controlled crystallinity for counter electrode in dye-sensitized solar cells. Sol Energy 85(11):2826–2832

10. Hwang S, Batmunkh M, Nine MJ et al (2015) Dye-sensitized solar cell counter electrodes based on carbon nanotubes. ChemPhysChem 16(1):53–65

11. Murakami TN, Ito S, Wang Q et al (2006) Highly efficient dye-sensitized solar cells based on carbon black counter electrodes. J Electrochem Soc 153(12):A2255

12. Banks CE, Davies TJ, Wildgoose GG et al (2005) Electrocatalysis at graphite and carbon nanotube modified electrodes: edge-plane sites and tube ends are the reactive sites. Chem Commun (Camb) 7:829–841

13. Veerappan G, Bojan K, Rhee SW (2011) Sub-micrometer-sized graphite as a conducting and catalytic counter electrode for dye-sensitized solar cells. ACS Appl Mater Interfaces 3(3):857–862

14. Liu GH, Wang H, Li X et al (2012) A mesoscopic platinized graphite/carbon black counter electrode for a highly efficient monolithic dye-sensitized solar cell. Electrochim Acta 69:334–339

15. Hosseinnezhad M, Shadman A, Rezaee B et al (2018) Tandem organic dye-sensitized solar cells: looking for higher performance and durability. Photonics Nanostruct Fundam Appl 31:34–43

16. Yamaguchi T, Uchida Y, Agatsuma S et al (2009) Series-connected tandem dye-sensitized solar cell for improving efficiency to more than 10%. Sol Energy Mater Sol Cells 93(6–7):733–736

17. Yanagida M, Onozawa-Komatsuzaki N, Kurashige M et al (2010) Optimization of tandem-structured dye-sensitized solar cell. Sol Energy Mater Sol Cells 94(2):297–302

18. Li GR, Wang F, Jiang QW et al (2010) Carbon nanotubes with titanium nitride as a low-cost counter-electrode material for dye-sensitized solar cells. Angew Chem Int Ed Engl 49(21):3653–3656

19. Guo JW, Zhang B, Hou Y et al (2013) A sulfur-assisted strategy to decorate MWCNTs with highly dispersed Pt nanoparticles for counter electrode in dye-sensitized solar cells. J Mater Chem A 1(6):1982–1986

20. González LM, Ramirez D, Jaramillo F (2022) Current status and trends of carbon-based electrodes for fully solution-processed perovskite solar cells. J Energy Chem 68:222–246

21. Hou Y, Wang D, Yang XH et al (2013) Rational screening low-cost counter electrodes for dye-sensitized solar cells. Nat Commun 4:1583

22. Wang D, Jiang J, Wang HF et al (2016) Revealing the volcano-shaped activity trend of triiodide reduction reaction: a DFT study coupled with microkinetic analysis. ACS Catal 6(2):733–741

23. Liu YF, Zhang XM, Li C et al (2019) Energy-level control via molecular planarization and its effect on interfacial charge-transfer processes in dye-sensitized solar cells. J Phys Chem C 123(22):13531–13537

24. Zheng ZW, Chen J, Hu Y et al (2014) Efficient sinter-free nanostructure Pt counter electrode for dye-sensitized solar cells. J Mater Chem C 2(40):8497–8500

25. Zhang B, Zhang NN, Chen JF et al (2013) Turning indium oxide into a superior electrocatalyst: deterministic heteroatoms. Sci Rep 3:3109

26. Omar A, Ali MS, Abd Rahim N (2020) Electron transport properties analysis of titanium dioxide dye-sensitized solar cells (TiO₂-DSSCs) based natural dyes using electrochemical impedance spectroscopy concept: a review. Sol Energy 207:1088–1121

27. Yu F, Shi Y, Yao WH et al (2019) A new breakthrough for graphene/carbon nanotubes as counter electrodes of dye-sensitized solar cells with up to a 10.69% power conversion efficiency. J Power Sources 412:366–373

28. Wu MX, Mu L, Wang YD et al (2013) One-step synthesis of nanoscaled tungsten oxides and carbides for dye-sensitized solar cells as counter electrode catalysts. J Mater Chem A 1(25):7519

29. Jin BB, Wang YF, Wang XQ et al (2016) Pulsed voltage deposited lead selenide thin film as efficient counter electrode for quantum-dot-sensitized solar cells. Appl Surf Sci 369:436–442

30. Wang W, Yao JX, Zuo XQ et al (2018) High efficiency nitrogen-doped core-shell carbon spheres as counter electrodes for dye-sensitized solar cells. Mater Lett 227:172–175

Wenjun Wu is an associate Professor at East China University of Science and Technology. He received his PhD degree from East China University of Science and Technology in 2008. From 2016 to 2017, he conducted his visiting scholar research in Prof. Neil Robertson's group at University of Edinburgh. His current research interests include dye-sensitized solar cells, carbon-based printable mesoscopic perovskite solar cells, and supercapacitors.